PAPER

Quantifying the interfacial load transfer in electrospun carbon nanotube polymer nanocomposite microfibers by using *in situ* Raman micromechanical characterization techniques

IOP Publishing Journal of Physics D: Applied Physics
J. Phys. D: Appl. Phys. **53** (2020) 365302 (13pp) https://doi.org/10.1088/1361-6463/ab8fdd

Quantifying the interfacial load transfer in electrospun carbon nanotube polymer nanocomposite microfibers by using *in situ* Raman micromechanical characterization techniques

Ohood Q Alsmairat[1,5], Feilin Gou[1,5], Christopher M Dmuchowski[1,2,5], Paul R Chiarot[1], Cheol Park[3], Ron N Miles[1] and Changhong Ke[1,4]

[1] Department of Mechanical Engineering, State University of New York at Binghamton, Binghamton, NY 13902, United States of America
[2] Materials Science and Engineering Program, State University of New York at Binghamton, Binghamton, NY 13902, United States of America
[3] Advanced Materials and Processing Branch, NASA Langley Research Center, Hampton, VA 23681, United States of America

E-mail: cke@binghamton.edu

Received 30 January 2020, revised 22 April 2020
Accepted for publication 4 May 2020
Published 23 June 2020

Abstract

The interfacial load transfer is of paramount importance to the bulk mechanical properties enhancement in nanotube-reinforced nanocomposites. Recent single-nanotube nanomechanical pull-out studies report quantitative interfacial load transfer characteristics of nanotube-matrix interfaces in close-to-ideal interfacial binding configurations. However, the elucidation of the actual interfacial load transfer in bulk nanotube nanocomposites remains a significant challenge due to the presence of many complex and inevitable nanotubes' conformational nonidealities, such as nanotube misalignment and aggregation/entanglement. Here we quantitatively investigate the interfacial load transfer in electrospun carbon nanotube poly(methyl methacrylate) (PMMA) nanocomposite microfibers by using *in situ* Raman micromechanical characterization techniques. The micromechanical measurements capture the critical tensile strain in the composite microfiber that initiates collective interfacial slip. The nanotube alignment inside the microfiber is characterized by using polarized Raman spectroscopy. The equivalent maximum interfacial shear stress in the tested nanotube-PMMA composite microfibers, which takes into account the nanotube alignment, is quantified using shear-lag micromechanics models and is found to be substantially lower than the reported values from single-nanotube pull-out measurements. The reported findings are helpful to better understand the effect of nanotube conformational nonidealities produced from processing on the interfacial stress transfer characteristics and the strengthening efficiency in nanotube-reinforced nanocomposites.

[4] Author to whom any correspondence should be addressed.
[5] These authors contributed equally to this work.

Supplementary material for this article is available online

Keywords: interfacial load transfer, carbon nanotubes, polymer nanocomposites, *in situ* Raman spectroscopy, polarized Raman spectroscopy

(Some figures may appear in colour only in the online journal)

1. Introduction

The light, strong, and tough properties of nanofiber-reinforced polymer nanocomposites are appealing to a number of engineering applications and industries [1]. The envisioned superior mechanical properties of these nanocomposites rely critically on effective interfacial load transfer on the nanofiber-matrix interface in order to make the most of the extraordinary structural and physical properties of reinforcing nanofillers, such as one-dimensional carbon and boron nitride nanotubes [2, 3] and two-dimensional graphene [4] and hexagonal boron nitride [5] nanosheets. This is because nanofillers have orders of magnitude larger surface to volume ratios as compared to microscale or macroscale fillers. Therefore, the mechanical strength of the nanofiber-matrix interface is of importance to the bulk mechanical property performance of nanofiber-reinforced nanocomposites [6, 7] and has been under intensive study for various nanofiber-reinforced polymer nanocomposite systems during the past two decades. From a scientific point of view, single-nanofiber pull-out tests [8] are ideal measurements to directly and quantitatively characterize the interfacial load transfer and the binding interaction on the interface of individual nanofibers with matrix materials, which is free of many nonidealities, such as fiber misalignment and aggregation/entanglement, inside the matrix. The tested nanofiber-matrix interface in composite specimens for single-nanofiber pull-out measurements is typically manufactured differently from those in traditional bulk nanocomposites, and only those individual and straight nanofibers in desired orientations are selected for pull-out measurements. Therefore, the quantitative single-nanofiber pull-out measurement data are useful to understand the interfacial load transfer and the molecular level binding interactions between nanofibers and matrix materials in a close-to-ideal interfacial binding configuration.

However, there are challenges and limitations of applying single-nanofiber pull-out measurements towards the study of the interfacial load transfer in nanotube nanocomposites. *First,* single-nanofiber pull-out experiments are highly challenging and have been conducted only by a handful of research groups worldwide. For instance, in single-nanotube pull-out experiments, it is desired that the embedded portion of a nanotube in a matrix stays straight and along the pulling force direction in order to avoid any bending effect. It is technically difficult to stretch the free end of the nanotube and to quantify the pulling force and monitor the mechanical response of the tested nanotube at sufficient force and spatial resolutions [9]. Due to these technical challenges, reports on direct, quantitative, and microscopic single-nanotube/fiber measurements of the interfaces in polymer nanocomposites reinforced by nanotubes or nanofibers remain quite limited [8–18], even after more than a decade of research. *Second,* the actual interfacial load transfer in bulk nanotube nanocomposites is influenced by the presence of the aforementioned complex and inevitable nanotubes' conformational nonidealities and may differ from those in single-nanotube pull-out measurements. It is well established that the nanotube alignment has a prominent influence on the bulk mechanical properties of nanotube composites. Only a fraction of loads can be transferred to and sustained by misaligned nanotubes as compared to those that are oriented perfectly along the stretching force direction, which leads to a reduction of their reinforcing efficiency. Due to their characteristics of large surface to volume ratios and high aspect ratios and the resulting strong inter-nanotube van der Waals interactions, even nanotubes that are fully dispersed and separated in solvent tend to aggregate and form entangled networks when mixed with polymer molecules, which is a long-standing and yet unsolved problem in the manufacturing of nanotube-polymer nanocomposites [19]. Aggregated/entangled nanotubes or nanotube networks may form vacancies and prevent a seamless contact on the nanotube-matrix interface, which results in a much weaker nanotube-matrix interface as compared to an ideal interfacial binding configuration with seamless contacts. It is noted that the nanotube misalignment alone does not alter the interfacial load transfer characteristics, but needs to be accounted for in order to evaluate how other nanotube nonidealities, such as nanotube aggregation/entanglement, influences the stress transfer on the nanotube-matrix interface. It is noted that substantial efforts have been made to extract and evaluate the interfacial load transfer from bulk mechanical measurements of nanofiber-reinforced polymer nanocomposites as well as measurements by using various microscopic and spectroscopy techniques, such as scanning electron microscopy (SEM) and transmission electron microscopy (TEM), Raman spectroscopy/microscopy, and atomic force microscopy (AFM) [20–26]. However, a vast majority of these bulk mechanical measurements and microscopic/spectroscopic characterization provide at most qualitative and indirect evaluation on the interfacial load transfer characteristics of nanofiber-reinforced polymer nanocomposites, which is in part due to the technical challenges in controlling and/or quantifying the nanotube alignment inside the matrix materials. The lack of scientific understanding of the interfacial load transfer on the nanofiller-matrix interface remains one of the major challenges in realizing the reinforcing potentials of these nanofillers in polymer nanocomposites, whose bulk performance remains substantially below the anticipated level based on the rule of mixtures [27].

In this paper, we quantitatively investigate the bulk interfacial load transfer characteristics of nanotube-reinforced

polymer nanocomposites by using *in situ* Raman micromechanical characterization techniques. A nanotube-polymer nanocomposite system that comprises double-walled carbon nanotubes (CNTs) and polymethyl methacrylate (PMMA) is employed in this study due to the wide-spread usage of this polymer composite system and the availability of their mechanical properties in the literature for the purpose of comparison [24]. In particular, the interfacial strength of CNT-PMMA nanocomposites has been previously investigated using single-nanotube pull-out techniques [18] as well as atomistic simulations [28]. The CNT-PMMA nanocomposite is manufactured in the form of microfibers using electrospinning techniques, which reportedly facilitate the nanotube alignment along the fiber axis as a result of the viscous flow of polymer solutions in the fiber manufacturing process [29, 30]. The interfacial load transfer in the electrospun nanotube composite fibers is quantified based on *in situ* Raman micromechanical measurements in conjunction with quantitative nanotube alignment measurements obtained using polarized Raman spectroscopy techniques. The equivalent maximum interfacial shear stress in the tested CNT-PMMA microfibers, which takes into account the nanotube alignment, is quantified using shear-lag micromechanics models and is found to be substantially lower than the reported values that were obtained from single-nanotube pull-out measurements. The presented experimental and theoretical methodologies can be readily extended to study the bulk interfacial load transfer characteristics of other nanotube-polymer composite systems, such as those reinforced with boron nitride nanotubes (BNNTs) [17, 31].

2. Materials and methods

2.1. Sample preparation

The employed PMMA (50 000 g mol^{-1} in molecular weight, purchased from Sigma-Aldrich Co.) was dissolved in acetone at a concentration of about 23%. The employed double-walled carbon nanotubes, which were acquired from Sigma-Aldrich Co., were manufactured using chemical vapour deposition methods with a purity of ∼65% and a length of ∼50 μm per the datasheet from the manufacturer. The diameters of CNTs were characterized by AFM in our prior studies and are found to be polydispersed and mostly within the range of 2.0–4.2 nm with 3.1 nm in median diameter [18]. The as-received nanotubes, which were in the form of dry powders, were first separated in dimethylformamide (DMF) using ultrasonication. The dispersed nanotube solution was then mixed with PMMA solutions to form two CNT-PMMA solutions with CNT weight concentrations of 0.1% and 0.5%, respectively. Microfibers were electrospun from pure PMMA solutions and CNT-PMMA solutions using an electro-spray printer [32, 33] with an applied voltage of 10 kV, a solution rate of about 10 μl min^{-1}, a glass nozzle size of 20–80 μm in diameter, and a nozzle-substrate separation of about 20 mm. The same CNT-PMMA solutions were also cast into thin-film control specimens. All of the manufactured polymer and composite microfiber and thin-film specimens were dried in a vacuum oven at room temperature for 12 h before mechanical and Raman measurements.

2.2. Sample characterization

The *in situ* Raman micromechanical characterization was conducted using a TST350 tensile tester from Linkam Scientific Instrument that is integrated with a Renishaw In-via Raman microscope using a 785 nm wavelength excitation laser, a grating of 1200 grooves per mm and a 0.55/50× objective lens. The tensile measurements were conducted at a strain rate of 1 mm s^{-1} and were held for about two minutes at each 0.25% strain mark for *in situ* Raman spectroscopy measurements. Polarized Raman spectroscopy measurements were conducted by using the same Renishaw Raman microscope that is equipped with polarization analyzers and a 785 nm laser. The scanning electron microscopy characterization was carried out using a Supra 55 SEM from Zeiss.

3. Results and discussion

3.1. In situ Raman micromechanical characterization of CNT-PMMA microfibers

Figure 1(a) illustrates the *in situ* Raman micromechanical characterization scheme. In this testing scheme, a doubly-clamped microfiber sample is incrementally stretched inside a tensile tester and a Raman laser beam is carefully positioned and focused on the outer surface of the strained fiber. Three types of microfibers were characterized in this study that included pure PMMA microfibers and two types of nanotube PMMA composite microfibers with CNT weight concentrations of 0.1% and 0.5%, respectively.

The tested microfibers were manufactured using electrospinning techniques [34], whose setup and operating principle are schematically illustrated in figure S1 (available online at stacks.iop.org/JPD/53/365302/mmedia) in supplementary materials and are briefly summarized here. The electrospinning setup is composed mainly of a syringe, a collecting substrate, and a high voltage power source [30]. There are also two electrodes in the system, one of which is attached to the substrate and the other one is inside the needle of the syringe and is in contact with the liquid solution. By applying a voltage between the two electrodes, an electric field is formed between the syringe needle and the substrate and the resulting electrostatic force drives the droplet to a conical shape droplet that is known as a Taylor cone [35] through balancing its surface tension. When the electrostatic force exceeds the surface tension force, the droplet is ejected from the needle tip toward the substrate and continuous fibers are thus formed and accumulated on the substrate. The added nanotubes, which are originally in random orientations, tend to orient along the liquid flow direction driven by the liquid viscous force inside the Taylor cone. It is noted that the electrospun fibers have a solid circular cross section and their diameters are controllable from sub-micron to ∼100 microns through adjusting the nozzle size of the syringe needle as well as the applied electric field. For ease of handing for mechanical testing, the

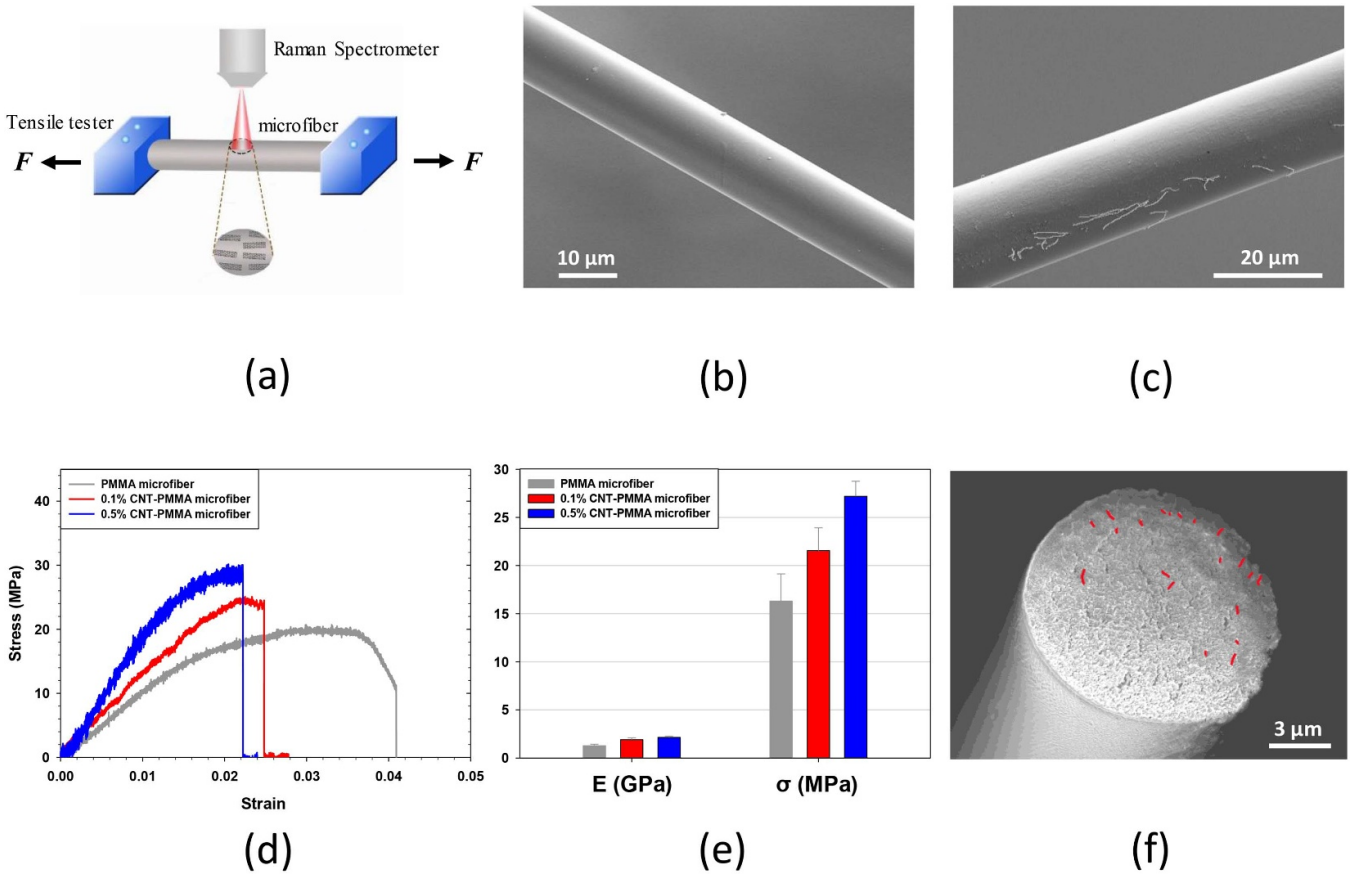

Figure 1. (a) Schematic of *in situ* Raman micromechanical characterization of nanotube-reinforced polymer nanocomposite fibers. (b) SEM image of one typical CNT-PMMA microfiber (0.1 CNT wt.%). (c) SEM image of one 0.5 wt.% CNT-PMMA fiber with several CNTs on the fiber's outer surface. (d) Representative stress–strain curves obtained on pure PMMA fibers and CNT-PMMA fibers. (e) The dependence of the microfiber's mechanical properties on the added CNT concentration. (f) SEM image of the fractured cross-sectional surface of one tested CNT-PMMA fiber that shows protruding nanotubes from interface debonding/pull-out (red coloring is added to aid visualization).

reported data in this paper are based on measurements that were conducted on microfibers of about 10–50 microns in diameter. Figure 1(b) shows an SEM image of one representative 0.1 wt.% CNT-PMMA microfiber. The SEM characterization shows that a majority of the manufactured microfibers have uniform circular cross sections and smooth surfaces. Occasionally, CNTs were also observed on the fiber's outer surface, as exemplified by the one shown in figure 1(c). A close examination reveals that those CNTs on the fiber's outer surfaces are preferably oriented along the fiber's longitudinal direction, which is direct evidence that the added CNTs possess a preferred orientation inside the electrospun fibers. Figure 1(c) also shows that the nanotubes are overall well-dispersed with varying lengths from a couple of microns to about 10 microns; however, it is also visible that some nanotubes aggregate and entangle together.

Figure 1(d) shows typical engineering stress-strain curves obtained on both pure PMMA fibers and CNT-PMMA fibers. The plots in figure 1(d) show that the added CNTs lead to a substantial increase of the Young's modulus and the ultimate tensile strength of the polymer fiber. The tensile measurement data based on six specimens of each type of fibers are summarized in figure 1(e) and also listed in table 1. The results show the pure PMMA fibers possess a Young's modulus of about 1.28 GPa and a tensile strength of about 16.31 MPa. The addition of 0.1 wt.% CNT results in an increase of the Young's modulus by about 49.1% to about 1.91 GPa and an increase of the ultimate tensile strength by about 32.1% to about 21.55 MPa. The addition of 0.5 wt.% CNT results in an increase of the Young's modulus by about 71.9% to about 2.2 GPa and an increase of the tensile strength by about 66.7% to about 27.19 MPa. The data show that both the Young's modulus and the tensile strength increase with CNT loading, but not in a linearly proportional manner. It is noticed that the ultimate tensile strain decreases with an increase in CNT loading. The SEM image displayed in figure 1(f) shows the fractured cross-sectional surface of one tested CNT-PMMA fiber with a number of sparsely distributed protruding nanotubes, which resulted from interface debonding and nanotube pull-out. Figures 1(d)–(f) clearly show that the effective interfacial load transfer on the CNT-polymer interface is responsible for the observed mechanical properties enhancement in the composites fibers.

During the sequential tensile loading, we also recorded the *in situ* Raman spectrum of the composite microfiber under test to understand the local interfacial loading characteristics of the embedded CNTs. Raman spectroscopy has been widely used to characterize the mechanical properties of CNT reinforced

Table 1. Summary of the experimentally measured and theoretically calculated parameters on the mechanical properties of CNT-PMMA microfibers.

	Pure PMMA fiber	0.1 wt.% CNT	0.5 wt.% CNT
Young's modulus (GPa, exp.)	1.28 ± 0.16	1.91 ± 0.18	2.2 ± 0.08
Ultimate stress (MPa, exp.)	16.31 ± 2.83	21.55 ± 2.37	27.19 ± 1.57
Critical strain (%, exp.)	—	1.11 ± 0.11	1.02 ± 0.03
Maximum IFSS (MPa, cal.)			
Gaussian distribution model	—	92 ± 9	94 ± 3
Step-function model	—	89 ± 9	83 ± 3

polymer composites [33]. Prior studies have demonstrated a reliable correlation between the mechanical strain in a CNT and the Raman peak shift of its characteristic bands [26]. Generally speaking, CNTs possess four primary characteristic bands in their Raman spectra (see figure S2): the Radial breathing mode (RMB) at 160–300 cm^{-1}, which is related with the symmetric movement of carbon atoms in CNTs in radial direction; the D band at 1250–1450 cm^{-1}, which originates from the defects in CNTs; the G band at 1500–1605 cm^{-1}, which is associated with the tangential vibrations of carbon atoms; and the 2D band at 2500–2700 cm^{-1}; which is the second-order mode of the D band [36]. When a uniaxial strain is applied to a CNT, the elongation of the covalent C-C bond results in a downward shift of its Raman G and 2D bands [37]. As shown in Figure S3, our studies reveal that the strain-induced downward shifts of these two bands show a similar trend, but the 2D band is more sensitive to strain change than the G band. Therefore, the Raman 2D band spectrum is employed here to characterize the local straining of CNTs inside the microfiber.

Figure 2(a) shows the typical Raman 2D band spectra of CNT-PMMA composite *fibers* that were recorded on a 0.1 wt.% CNT-PMMA microfiber under zero and a 1.5% strain. The applied strain results in a downshift of about 20 cm^{-1} in the CNT's 2D band peak frequency. As a comparison, typical Raman 2D band spectra of 0.1 wt.% CNT-PMMA composite *films* are also displayed in figure 2(a), which shows a downshift 2D band peak frequency of about 10 cm^{-1}. The results clearly indicate that the interfacial load transfer between CNTs and polymer matrices are more effective in fiber samples than in film samples, even though they are essentially made from the same composite materials.

It is noted that the recorded Raman spectrum and the observed characteristic Raman band peak frequency shift are based on the collective scattered Raman signals from all the nanotubes that are inside the light–matter interaction volume. Here we estimate the number of nanotubes inside the interaction volume based on the laser beam spot diameter ($=1.22\lambda/\mathrm{NA}$), where λ is the wavelength of the laser beam and NA is the numerical aperture of the employed microscope objective. For a 785-nm laser and a 0.55/50x objective, the laser spot diameter is calculated to be about 1.9 μm. By assuming the interaction volume as a semisphere and nanotubes of 3.1 nm in outer diameter, the number of nanotubes inside the interaction volume is calculated to be about 125 (625) for 0.1 (0.5) wt.% CNT-PMMA fibers. Because the nanotubes have diverse orientations in the fiber, the mechanical strains inside the nanotubes vary. It is noted that the strain in a nanotube is a cosine function of its orientation angle to the fiber axis or the applied tensile force direction. The recorded Raman spectra as shown in figure 2(a) show the aggregate Raman signal through superimposing the scattered signals from all the nanotubes that interact with the laser beam, as illustrated in figure 2(b). Therefore, the peak frequency corresponds to those nanotubes under median strains.

Figure 2(c) shows representative 2D band peak frequency shift as a function of the applied strain for both 0.1 wt.% and 0.5 wt.% CNT-PMMA composites fibers. The data show a consistent downshift of the peak frequency, in a nearly linear trend, with an increase in strain and then the peak frequency formed a plateau even with substantial further strain increases. The downshift of the 2D band peak frequency can be attributed to increasingly straining of CNTs in the microfiber through the interfacial load transfer on the CNT–polymer interface and the resulting weakening of C–C bond interactions due to the bond elongation [38–41].

The observed plateau shows that the strain in the CNTs reaches an overall saturated stage and the interfacial load transfer on the CNT–polymer interface reaches its physical limits, which indicates that slip occurs on the CNT–polymer interface. We fit the measured 2D band peak frequency shift curves by using a bilinear fitting curve that comprises a linear segment for small strains and a constant segment for large strains. The strain at the junction of the two fitting segments is considered a critical strain in the fiber where the CNT–polymer interface starts to slip. The critical strain for 0.1 wt.% CNT-PMMA fibers is found to be $1.11 \pm 0.11\%$, while $1.02 \pm 0.03\%$ for 0.5 wt.% CNT-PMMA fibers, based on measurements of five specimens of each type of fibers. It is noted that the measured critical strain coincides well with the proportional strain limit (i.e. the strain at the end of the linear segment in the stress-strain curve) in the recorded stress-strain curves of the composite microfibers shown in figure 1(d). This observation suggests that the nonlinear stress–strain behavior in the composite fiber, which is beyond the initial linear segment, is accompanied by interfacial slips on CNT-polymer interfaces.

The full width at half maximum (FWHM) of the recorded Raman 2D band spectra is also measured, as exemplified by the inset plot in figure 2(c), and is found to remain in a narrow range, which indicates a uniform stress distribution inside the nanotubes during the stretching process [26]. Scattering of the Raman peak frequency data is exhibited in figure 2(b) and can be attributed to a few sources, such as the multi-walled

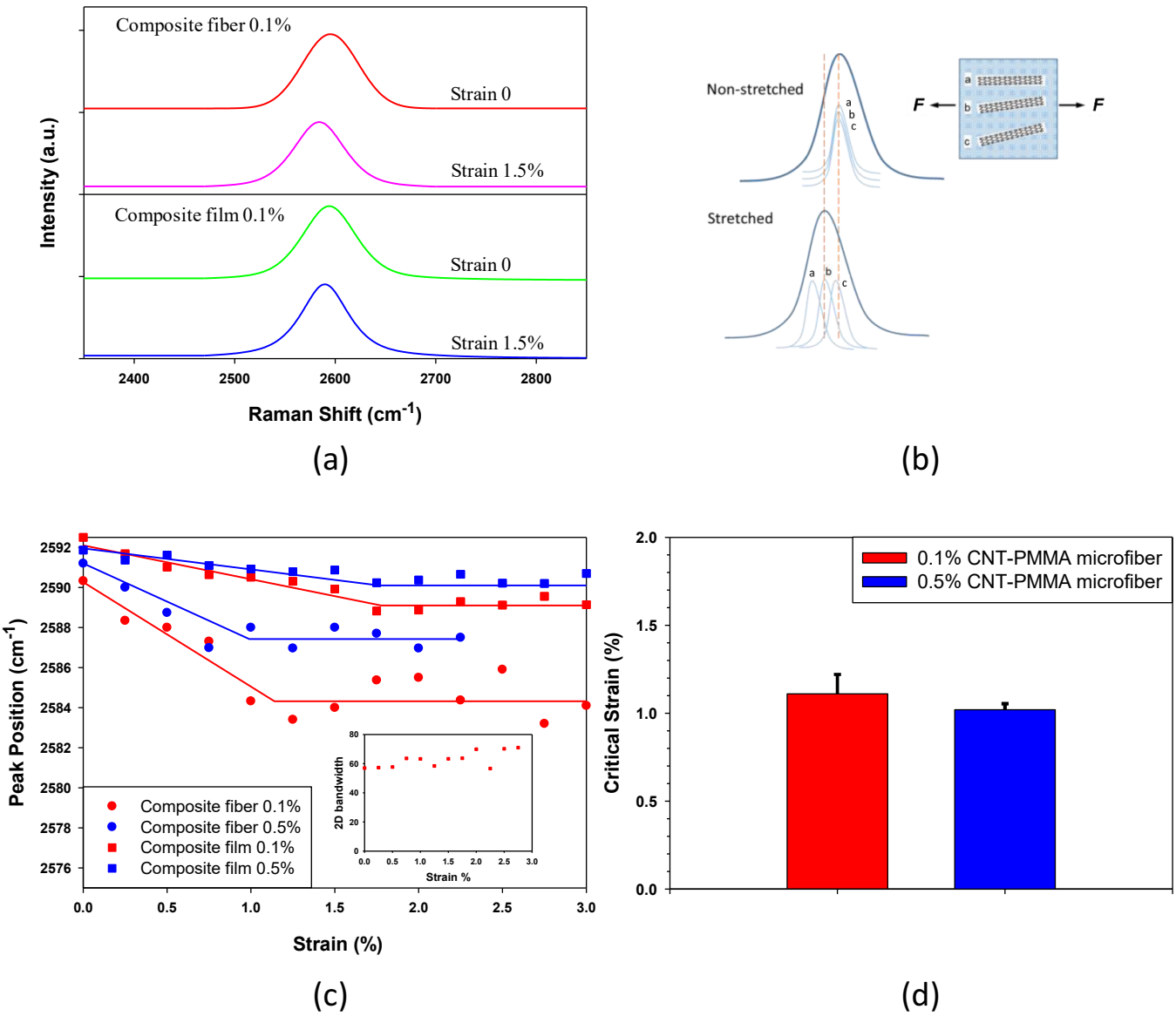

Figure 2. (a) Representative *in situ* Raman spectra of 0.1 wt.% CNT-PMMA fibers (top) and films (bottom) under zero and 1.5% strain. (b) Schematic of strain-induced Raman peak shift in nanotube composites; (c) representative *in situ* Raman CNT 2D band peak frequency shift as a function of strain. The circle-dotted (square-dotted) curves are experimental measurements recorded on two CNT-PMMA fiber (film) samples (red: 0.1 wt.% and blue: 0.5 wt.%). The solid curves are the bilinear fitting curves to the respective measurement data sets. (d) The quantified critical strains for the tested CNT-PMMA fibers.

characteristics of the employed nanotubes [42], misalignment of the nanotubes in the fiber [43], and the uncertainties in positioning and focusing the laser beam onto the same spot on the fiber surface during the *in situ* measurements.

For the electrospun nanotube composite fibers, the nanotubes are preferably aligned along the fiber axis direction, which is confirmed by our polarized Raman measurements (see section 3.2 for details). In contrast, the nanotubes are randomly oriented in comparable composite film specimens. It is expected that a fiber specimen should possess a much lower critical strain than a comparable film specimen, which is confirmed by the control experimental data shown in figure 2(c). The critical strains in 0.1 wt.% and 0.5 wt.% CNT-PMMA film specimens are quantified to be about 1.7% and about 1.8%, respectively. The results further show that the measured Raman peak frequency shift is an indication of the interfacial load transfer in the CNT–polymer composites.

3.2. Quantification of the nanotube alignment in microfibers by using polarized Raman spectroscopy

The *in situ* Raman measurements indicate that nanotubes have better alignment in microfiber specimens than in film specimens and the tube alignment in microfibers is also affected by the CNT concentration. In order to obtain the interfacial load transfer characteristics of CNT-polymer microfibers, it is essential to quantify the nanotube alignment inside such fibers. Here we quantify the nanotube alignment in microfibers by using polarized Raman spectroscopy. In general, polarized Raman spectroscopy provides information

about the molecular orientation of the bond vibration, in addition to the typical chemical information provided by regular Raman spectroscopy.

Due to the one-dimensional characteristics of CNTs, their Raman scattering intensities exhibit orientation dependencies [44]. The polarized Raman spectroscopy techniques have been previously employed in probing the nanotube alignment in bundled fibers [45] and polymer nanocomposites [46, 47]. Gommans *et al* [48] reported that the Raman scattering intensity (vertical/vertical (*VV*) polarizers) of the polarization geometry with a parallel analyzer is dependent upon the sample angle with respect to incident polarized light (φ), which is given as $VV(\varphi) \propto \cos^4(\varphi)$. For a CNT-polymer fiber geometry as illustrated in figure 3(a), given a certain fiber orientation angle φ with respect to the incident laser beam, the intensity of the CNT's characteristics band peak is proportional to:

$$VV(\varphi) \propto p \int_{\varphi-\theta}^{\varphi+\theta} \cos^4(\varphi) d\varphi + (1-p) \int_{\varphi+\theta}^{\pi+\varphi-\theta} \cos^4(\varphi) d\varphi, \quad (1)$$

where p is the mole fraction of the nanotubes that lie within $\pm\theta$ of the fiber axis, while the remainder $(1-p)$ are distributed among all other outside angles, which range from θ *to* $\pi-\theta$. Assuming that the nanotubes are preferably oriented along the fiber axis direction, the intensities for all CNT's characteristics bands should diminish with an increasing fiber orientation angle φ. Here we pick the G band of CNTs (peak frequency $\sim$1592 cm^{-1}) to characterize their alignment in microfibers because their G band spectra possess the highest intensities among all of their characteristic bands (see figure S2).

For both 0.1 wt.% and 0.5 wt.% CNT-PMMA microfibers, polarized Raman measurements were taken at certain selected angles with respect to the incident polarization as shown in figure 3(a). Repeat acquisitions were obtained to account for both local variations in CNT concentration and CNT alignment within the fiber, and sample landmarks were used to ensure consistency when the fiber was rotated. The selected typical polarized Raman spectra displayed in figure 3(b), which were recorded on a 0.5 wt.% microfiber, show the G band peak intensity diminishes at increasing angles with respect to the incident light. It is noted that only Raman peaks associated with the C-C bonds in CNTs diminish in proportions as predicted by the model described above, while those bands associated with chemical bonds in polymer chains remain independent of the orientation change. Figure 3(c) shows the dependence of the recorded intensity of the G band peak frequency on the fiber orientation measured on a 0.5 wt.% microfiber. As a control, polarized Raman spectroscopy measurements were also conducted on CNT-PMMA *film* specimens, as exemplified by the inset plot in figure 3(c). As expected, the intensity of the G band peak for the film sample remains largely independent of the orientation angle, which indicates that the added nanotubes do not possess any preferred orientation alignment inside the composite film. The measurement results shown in figure 3(c) clearly demonstrate that the nanotubes in electrospun microfibers are preferably aligned along the fiber axis direction. The measured peak intensity data points for microfiber specimens are curve fitted using equation (1) to obtain the values of p and θ. From the data shown in figure 3(c), p and θ are found to be about 95.4% and 17° respectively for the tested 0.5 wt.% microfiber. We have performed a number of polarized Raman spectroscopy measurements on the CNT-PMMA microfiber specimens and the alignment results based on six specimens of each CNT concentration are displayed in figure 3(d) and also listed in table 2. For the 0.1 wt.% CNT-PMMA microfibers, θ is found to range from 7° to 14° with a mean value of about 10.3° and a standard deviation of 2.3°. In comparison, the 0.5 wt.% CNT-PMMA microfibers are found to possess a much higher nanotube alignment angle ($\theta = 21.3 \pm 3.3°$). The results clearly demonstrate that the nanotubes are overall more preferably aligned along the fiber axis in microfibers with lower nanotube concentrations, which can be attributed to a larger separation of nanotubes in lower nanotube concentration polymer solutions and weaker inter-nanotube interactions during the viscous force-driven nanotube alignment process. It is noted that the measured nanotube alignment by using polarized Raman spectroscopy is consistent with prior reports by using small-angle x-ray scattering (SAXS) [26].

It is noted the nanotube alignment data that are obtained from the analysis of the polarized Raman spectroscopy measurements are still in a collective form. In order to employ such data to evaluate the interfacial load transfer characteristics of CNT-PMMA microfibers, we have to make assumptions about the nanotube distribution profiles. Here we consider two distribution models: (1) Gaussian (or normal) distribution: the orientations of all the nanotubes in a fiber are assumed to follow a Gaussian distribution within the angle of 0 to 90°. Figure 3(e) shows the nanotube orientation distribution profile by using this Gaussian distribution model based on the polarized Raman measurement shown in figure 3(c) with a probability-weighted mean nanotube alignment angle of about 6.7°. Using the nanotube alignment data shown in figure 3(d), the probability-weighted nanotube alignment angle is found to be 3.6° ± 1.1°(0.1 wt.%) and 8.4° ± 1.8° (0.5 wt.%), respectively, both of which are displayed in figure 3(f) and also listed in table 2. (2) Step-function distribution: the orientations of all the nanotubes are assumed to be either the value of θ that is obtained from curve fitting of the polarized Raman measurements or 90°, the latter of which implies that these tubes are aligned perpendicular to the fiber axis and does not contribute to the polarized Raman band intensity. Therefore, all the nanotubes are assumed to be oriented with the same angle of θ (i.e. $\theta = 10.3° \pm 2.3°$ (21.3° ± 3.3°) in 0.1 wt.% (0.5 wt.%) fibers) under this step-function distribution model. It is clear that the Gaussian distribution model gives a much smaller average nanotube alignment angle as compared to the step-function model, while the step-function model provides an upper limit on the possible nanotube alignment angle in a fiber.

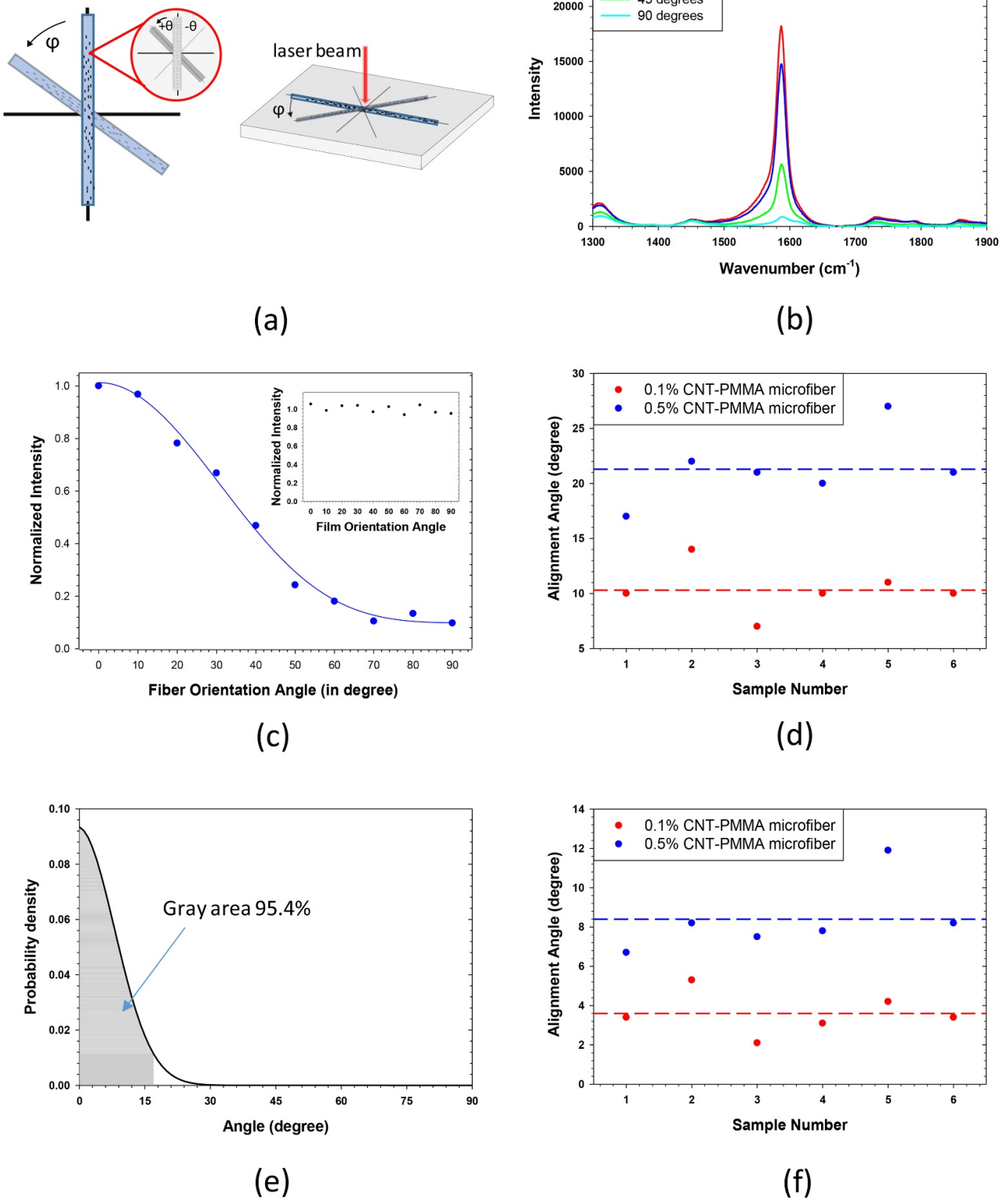

Figure 3. Quantification of the nanotube alignment inside the electrospun nanocomposite fibers by using polarized Raman spectroscopy: (a) schematic of polarized Raman experimental setup on a nanotube-polymer fiber with varying orientation angles. (b) Polarized Raman spectra of one 0.5 wt.% CNT-PMMA composite fiber recorded at selected orientation angles. (c) The dependence of the CNT peak intensity at 1590 cm^{-1} on the fiber orientation angle recorded for one 0.5 wt.% CNT-PMMA composite fiber. The solid curve is the fitting curve by using equation (1). (d) Calculated alignment angle θ of CNTs along the axial direction of CNT-PMMA fibers. (e) Prediction of the nanotube alignment angle distribution based on the Gaussian distribution model for the tested microfiber shown in (d). (f) Probability-weighted average nanotube alignment angle. The dashed lines in (d) and (f) indicate the average values of the respective data sets.

Table 2. Summary of the nanotube alignment measurements in CNT-PMMA microfibers by using polarized Raman spectroscopy.

	0.1 wt.% CNT			0.5 wt.% CNT		
Sample #	p (%)	θ (°)	Probability-weighted average angle—Gaussian distribution model (°)	p (%)	θ (°)	Probability-weighted average angle—Gaussian distribution model (°)
1	97.96	10	3.4	95.4	17	6.7
2	96.42	14	5.3	96.42	22	8.2
3	98.98	7	2.1	97.45	21	7.5
4	98.98	10	3.1	95.92	20	7.8
5	96.43	11	4.2	92.86	27	11.9
6	97.96	10	3.4	95.92	21	8.2
Average	97.79 ± 1.15	10.3 ± 2.3	3.6 ± 1.1	95.66 ± 1.54	21.3 ± 3.3	8.4 ± 1.8

3.3. Quantification of the interfacial load transfer characteristics of CNT-PMMA microfibers

The polarized Raman spectroscopy measurement results indicate that the orientation of the nanotube fillers in a microfiber specimen is polydispersed, as illustrated by the left drawing in figure 4(a). In order to obtain the overall local interfacial load transfer characteristics of CNT-PMMA microfibers, we first obtain an equivalent nanotube-polymer composite system in which all the nanotube fillers are assumed to possess the same orientation angle, as illustrated by the right drawing in figure 4(a). The equivalent nanotube orientation angle with respect to the fiber axis, α, is assumed to be the experimental-informed nanotube alignment angle from polarized Raman measurements. Figure 4(b) illustrates an equivalent single-nanotube composite configuration in which a nanotube of a diameter D_{nt} and a length $2l$ is concentrically embedded into a same-length cylindrical polymer matrix with an outer diameter of D_m, and inter-nanotube interactions are assumed to be negligible due to low nanotube concentrations. This equivalent single-nanotube composite configuration in conjunction with the adoption of the same continuum mechanics model will facilitate the comparison of the interfacial shear stress (IFSS) values obtained from this study with previously reported values obtained based on single-nanotube pull-out measurements. Prior studies show that the IFSS distribution on the CNT-polymer interface is governed by the shear lag effect and is highly non-uniform in nature. The IFSS possesses its maximum at the nanotube ends and starts to decreases toward the central interface region. With the nanotube under an axial stretching force F that is transferred via the CNT-PMMA interface, the shear stress on the CNT-PMMA interface is given as [49]

$$\tau = \frac{F \cdot n}{2A_{nt}} \frac{\cosh\left(2n \cdot x/D_{nt}\right)}{\sinh\left(2n \cdot l/D_{nt}\right)}, \tag{2}$$

where x is the coordinate along the nanotube axial direction with $x = 0$ at the nanotube middle length point, A_{nt} is the nanotube's cross-sectional area, and n is given by $n = \sqrt{\frac{E_m}{E_{nt} \cdot (1+\nu_m) \cdot \log(D_m/D_{nt})}}$, in which E_m and ν_m are the Young's modulus and the Poisson's ratio of the matrix, respectively.

In the equivalent CNT-PMMA microfiber configuration as shown in figure 4(b), with the microfiber under an axial strain of ε, the axial force exerted on the nanotube is given by

$$F = A_{nt} E_{nt} \varepsilon \cos^2\alpha, \tag{3}$$

where E_{nt} is the Young's modulus of CNTs

When the axial strain in the microfiber reaches the critical strain ε_{cr}, the IFSS on the CNT-PMMA interface reaches its maximum at the nanotube ends (i.e. $x = \pm l$), which is given as,

$$\tau_{max} = \frac{E_{nt} \varepsilon_{cr} \cos^2\alpha \cdot n}{2 \cdot \tanh\left(2n \cdot l/D_{nt}\right)}. \tag{4}$$

Based on the measured critical strain ε_{cr} (see table 1) and the p-valued weighted average nanotube alignment angle (see table 2), the equivalent τ_{max} in the microfibers is calculated and listed in table 1. The calculations are based on the following parameters: $E_m = 1.28$ GPa; $\nu_m = 0.32$; $D_{nt} = 3.1$ nm; $E_{nt} = 1$ TPa [18] and $l = 1000$ nm. Furthermore, the diameter of the polymer cylinder in the single-nanotube composite configuration D_m is calculated to be about 105 nm (47 nm) for 0.1 (0.5) wt.% CNT-PMMA fibers by considering a density of 1.18 g cm^{-3} for PMMA and a density of 1.35 g cm^{-3} for CNTs. It is noted that τ_{max} becomes independent of l when l exceeds a certain value, which is found to be about 500 nm based on the parameters used here. The equivalent τ_{max} is found to be about 92 MPa (0.1 wt.%) and about 94 MPa (0.5 wt.%) based on the nanotube alignment angle from the Gaussian distribution model, both of which are higher than the respective values (i.e. 89 MPa and 83 MPa) obtained based on that from the step function model. The results show that the nanotube concentration does not have a significant impact on the equivalent τ_{max}, which indicates that the IFSS that is quantified with the correction of the nanotube misalignment is on par for the two types of composite fibers tested in this study. It is noted that the level of the interfacial shear stress on CNT-PMMA interfaces obtained in this study as well as our prior single-nanotube pull-out study could not be fully attributed to weak van der Waals interactions. Therefore, our results suggest the existence of strong chemical bonds on the nanotube–polymer interface, such as covalent bonding predicted by Bagchi *et al* [50]. In addition, the effect of the nanotube alignment angle on the bulk mechanical properties of the composite is shown in equation (3) that the transferred load to the nanotube via the nanotube-polymer interface is linearly proportional to the cosine-squared function of the nanotube

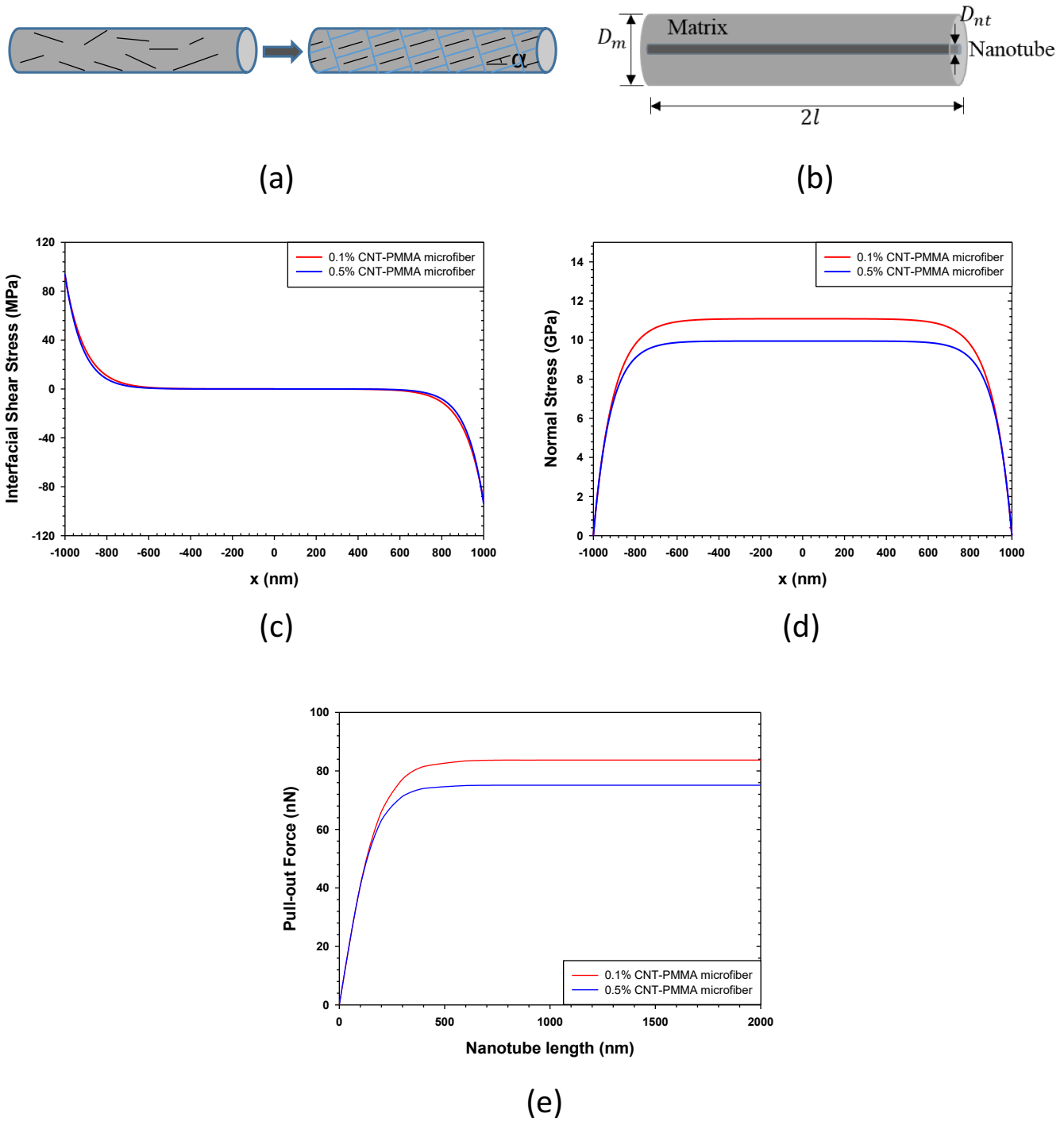

Figure 4. (a) Schematics of the general configuration of a short-nanotube polymer composite fiber (left) and its equivalent configuration (right). (b) Schematic of the single-nanotube polymer composite configuration. (c), (d) Theoretically predicted (c) interfacial shear stress distribution and (d) normal stress distribution on the CNT-polymer interface in the equivalent nanotube-polymer composite fiber. The nanotube length and diameter are assumed to be 2000 nm and 3.1 nm respectively in the calculation. (e) The dependence of the theoretically calculated maximum CNT-polymer interface load on the embedded nanotube length.

alignment angle. Therefore, the decent nanotube alignments in the tested microfibers in this study have a positive contribution to the observed Young's modulus and strength enhancements of the composite microfibers.

The pointwise IFSS distribution profiles along the nanotube axis on the onset of the interfacial slip are shown in figure 4(c), while the corresponding normal stress distribution is shown in figure 4(d), by assuming $l = 1000$ nm and using the p-value weighted nanotube angle obtained from the Gaussian distribution model. The results show a quite rapid decay in the nanotube end region and the effective load transfer occurs only at a length of about 400 nm at each tube end. In

contrast to the IFSS, the maximum normal stress in the nanotube occurs in the central tube segment and is found to be about 11.1 GPa (10.0 GPa) for 0.1 (0.5) wt.% CNT-PMMA fibers. Our analysis shows that the maximum load that can be transferred on the nanotube-polymer interface is dependent on the nanotube's embedded length, as displayed in figure 4(e). The results show that the maximum interfacial load first increases with the nanotube length and then reaches a saturated level. Therefore, it is of advantage to use sufficiently long nanotubes in composites in order to achieve better interfacial load transfer and thus bulk mechanical properties.

As a comparison, recent single-nanotube pull-out experimental studies that used an *in situ* nanomechanical characterization technique report a value of about 155 MPa for CNT-PMMA interfaces, which is substantially higher than the values obtained in the present study. The results show the equivalent maximum IFSS in the microfibers with decent nanotube alignment remains substantially lower (∼41–54%) than the ideal value. The lower interfacial load transfer in the nanotube composite microfiber can be attributed to nanotube dispersion/separation issues, such as nanotube aggregation and entanglements, which are evidenced by the nanotubes staying on the outer surface of the microfiber (figure 1(c)). Even though the importance of the nanotube alignment and dispersion/separation on the mechanical property enhancement of nanotube-polymer nanocomposites has been well documented in the literature [51], the present study is among the first to report quantitative assessment on the substantial impact of nanotube's conformational nonidealities produced from nanotube and composite processing on the local interfacial load transfer characteristics. The findings here further emphasize the necessity of avoiding or minimizing the nanotube nonidealities in the manufacturing of nanotube-polymer composites in order to maximize the reinforcing potentials of nanotube fillers in the bulk mechanical properties of nanotube composites. We want to highlight that the polymer nanocomposite microfibers with enhanced and tunable mechanical properties can be useful for a wide range of applications, such as raw materials for functional fabrics [52] and air flow sensing elements in hearing aid devices [53].

4. Conclusion

The bulk interfacial load transfer characteristics of electrospun carbon nanotube-polymer nanocomposite microfibers are investigated using an *in situ* Raman micromechanical characterization technique in conjunction with polarized Raman spectroscopy measurements. The results reveal that the nanotube concentration in the composite fiber has a noticeable influence on the nanotube alignment, but has much less impact on the local interfacial stress transfer. The maximum interfacial shear stress in the microfiber that is obtained by taking into account the nanotube misalignment is substantially lower than the reported values obtained from single-nanotube pull-out experiments. The results reveal that the interfacial load transfer characteristics are substantially influenced by those processing-induced nanotube nonidealities, such as nanotube aggregation and entanglement. The presented experimental and theoretical methodologies are readily applicable to study the bulk interfacial load transfer characteristics of other nanotube composites systems. The reported findings are helpful to better understand the effect of nanotube misalignment and other nanotube conformational nonidealities produced from processing on the interfacial stress transfer characteristics and the strengthening efficiency in nanotube-reinforced nanocomposites.

Acknowledgments

This work was supported by the US Air Force Office of Scientific Research—Low Density Materials program under Grant No. FA9550-15-1-0491, by the National Science Foundation under Grant No. CMMI-1537333, and by the National Institute of Health under Grant No. 1R01DC017720. The AFM and Raman spectroscopy measurements were performed using a facility that was acquired through an NSF-MRI Award (CMMI-1429176). P R C acknowledges the National Science Foundation for support of the electrospray printer (CMMI-1554038). C M D acknowledges fellowship support from the New York NASA Space Grant Consortium.

ORCID iD

Changhong Ke https://orcid.org/0000-0002-5170-9859

References

[1] Baur J and Silverman E 2011 Challenges and opportunities in multifunctional nanocomposite structures for aerospace applications *MRS Bull.* **32** 328–34
[2] Iijima S 1991 Helical microtubules of graphitic carbon *Nature* **354** 56–8
[3] Chopra N G, Luyken R J, Cherrey K, Crespi V H, Cohen M L, Louie S G and Zettl A 1995 Boron-nitride nanotubes *Science* **269** 966–7
[4] Novoselov K S, Geim A K, Morozov S V, Jiang D, Zhang Y, Dubonos S V, Grigorieva I V and Firsov A A 2004 Electric field effect in atomically thin carbon films *Science* **306** 666–9
[5] Bosak A, Serrano J, Krisch M, Watanabe K, Taniguchi T and Kanda H 2006 Elasticity of hexagonal boron nitride: inelastic x-ray scattering measurements *Phys. Rev.* B **73** 041402
[6] Zhang Y, Song K, Meng J and Minus M L 2013 Tailoring polyacrylonitrile interfacial morphological structure by crystallization in the presence of single-wall carbon nanotubes *ACS Appl. Mater. Interfaces* **5** 807–14
[7] Tao X, Dong L, Wang X, Zhang W, Nelson B J and Li X 2010 B4C-nanowires/carbon-microfiber hybrid structures and composites from cotton T-shirts *Adv. Mater.* **22** 2055–9
[8] Cooper C A, Cohen S R, Barber A H and Wagner H D 2002 Detachment of nanotubes from a polymer matrix *Appl. Phys. Lett.* **81** 3873–5
[9] Chen X, Zhang L, Zheng M, Park C, Wang X and Ke C 2015 Quantitative nanomechanical characterization of the van der Waals interfaces between carbon nanotubes and epoxy *Carbon* **82** 214–28

[10] Barber A H, Cohen S R, Kenig S and Wagner H D 2004 Interfacial fracture energy measurements for multi-walled carbon nanotubes pulled from a polymer matrix *Compos. Sci. Technol.* **64** 2283–9

[11] Ozkan T, Chen Q and Chasiotis I 2012 Interfacial strength and fracture energy of individual carbon nanofibers in epoxy matrix as a function of surface conditions *Compos. Sci. Technol.* **72** 965–75

[12] Manoharan M P, Sharma A, Desai A V, Haque M A, Bakis C E and Wang K W 2009 The interfacial strength of carbon nanofiber epoxy composite using single fiber pullout experiments *Nanotechnology* **20** 295701

[13] Tsuda T, Ogasawara T, Deng F and Takeda N 2011 Direct measurements of interfacial shear strength of multi-walled carbon nanotube/PEEK composite using a nano-pullout method *Compos. Sci. Technol.* **71** 1295–300

[14] Ganesan Y, Peng C, Lu Y, Loya P E, Moloney P, Barrera E, Yakobson B I, Tour J M, Ballarini R and Lou J 2011 Interface toughness of carbon nanotube reinforced epoxy composites *ACS Appl. Mater. Interfaces* **3** 129–34

[15] Barber A H, Cohen S R and Wagner H D 2003 Measurement of carbon nanotube–polymer interfacial strength *Appl. Phys. Lett.* **82** 4140

[16] Barber A H, Cohen S R, Eitan A, Schadler L S and Wagner H D 2006 Fracture transitions at a carbon-nanotube/polymer interface *Adv. Mater.* **18** 83–87

[17] Chen X, Zhang L, Park C, Fay C C, Wang X and Ke C 2015 Mechanical strength of boron nitride nanotube-polymer interfaces *Appl. Phys. Lett.* **107** 253105

[18] Chen X, Zheng M, Park C and Ke C 2013 Direct measurements of the mechanical strength of carbon nanotube–poly(methyl methacrylate) interfaces *Small* **9** 3345–51

[19] Huang Y Y and Terentjev E M 2008 Dispersion and rheology of carbon nanotubes in polymers *Int. J. Mater. Form.* **1** 63–74

[20] Nautiyal P, Rudolf C, Loganathan A, Zhang C, Boesl B and Agarwal A 2016 Directionally aligned ultra-long boron nitride nanotube induced strengthening of aluminum-based sandwich composite *Adv. Eng. Mater.* **18** 1747–54

[21] Yamaguchi M, Meng F, Firestein K, Tsuchiya K and Golberg D 2014 Powder metallurgy routes toward aluminum boron nitride nanotube composites, their morphologies, structures and mechanical properties *Mater. Sci. Eng.* A **604** 9–17

[22] Lahiri D, Hadjikhani A, Zhang C, Xing T, Li L H, Chen Y and Agarwal A 2013 Boron nitride nanotubes reinforced aluminum composites prepared by spark plasma sintering: microstructure, mechanical properties and deformation behavior *Mater. Sci. Eng.* A **574** 149–56

[23] Yamaguchi M, Pakdel A, Zhi C, Bando Y, Tang D-M, Faerstein K, Shtansky D and Golberg D 2013 Utilization of multiwalled boron nitride nanotubes for the reinforcement of lightweight aluminum ribbons *Nanoscale Res. Lett.* **8** 3

[24] Singhal S K, Srivastava A K, Pasricha R and Mathur R B 2011 Fabrication of Al-matrix composites reinforced with amino functionalized boron nitride nanotubes *J. Nanosci. Nanotechnol.* **11** 5179–86

[25] Xue Y *et al* 2015 Aluminum matrix composites reinforced with multi-walled boron nitride nanotubes fabricated by a high-pressure torsion technique *Mater. Des.* **88** 451–60

[26] Mu M, Osswald S, Gogotsi Y and Winey K I 2009 Anin situRaman spectroscopy study of stress transfer between carbon nanotubes and polymer *Nanotechnology* **20** 335703

[27] Coleman J N, Khan U, Blau W J and Gun'ko Y K 2006 Small but strong: a review of the mechanical properties of carbon nanotube–polymer composites *Carbon* **44** 1624–52

[28] Zheng Q, Xue Q, Yan K, Gao X, Li Q and Hao L 2008 Influence of chirality on the interfacial bonding characteristics of carbon nanotube polymer composites *J. Appl. Phys.* **103** 044302

[29] Yeo L Y and Friend J R 2006 Electrospinning carbon nanotube polymer composite nanofibers *J. Exp. Nanosci.* **1** 177–209

[30] Jiang S, Chen Y, Duan G, Mei C, Greiner A and Agarwal S 2018 Electrospun nanofiber reinforced composites: a review *Polym. Chem.* **9** 2685–720

[31] Chang H, Lu M, Arias-Monje P J, Luo J, Park C and Kumar S 2019 Determining the orientation and interfacial stress transfer of boron nitride nanotube composite fibers for reinforced polymeric materials *ACS Appl. Nano Mater.* **2** 6670–6

[32] Brown N A, Zhu Y, German G K, Yong X and Chiarot P R 2017 Electrospray deposit structure of nanoparticle suspensions *J. Electrost.* **90** 67–73

[33] Zhu Y and Chiarot P R 2019 Structure of nanoparticle aggregate films built using pulsed-mode electrospray atomization *J. Mater. Sci.* **54** 6122–39

[34] Boys C V 1887 On the production, properties, and some suggested uses of the finest threads *Proc. Phys. Soc. Lond.* **9** 8–19

[35] Melcher J R and Taylor G I 1969 Electrohydrodynamics: a review of the role of interfacial shear stresses *Annu. Rev. Fluid Mech.* **1** 111–46

[36] Gao Y, Li L, Tan P, Liu L and Zhang Z 2010 Application of Raman spectroscopy in carbon nanotube-based polymer composites *Chin. Sci. Bull.* **55** 3978–88

[37] Cronin S B, Swan A K, Ünlü M S, Goldberg B B, Dresselhaus M S and Tinkham M 2005 Resonant Raman spectroscopy of individual metallic and semiconducting single-wall carbon nanotubes under uniaxial strain *Phys. Rev.* B **72** 035425

[38] Cronin S B, Swan A K, Unlü M S, Goldberg B B, Dresselhaus M S and Tinkham M 2004 Measuring the uniaxial strain of individual single-wall carbon nanotubes: resonance Raman spectra of atomic-force-microscope modified single-wall nanotubes *Phys. Rev. Lett.* **93** 167401

[39] Cooper C A, Young R J and Halsall M 2001 Investigation into the deformation of carbon nanotubes and their composites through the use of Raman spectroscopy *Compos. Part Appl. Sci. Manuf.* **32** 401–11

[40] Zhao Q and Wagner H D 2004 Raman spectroscopy of carbon-nanotube-based composites *Phil. Trans.* A **362** 2407–24

[41] Wu G, Zhou J and Dong J 2005 Raman modes of the deformed single-wall carbon nanotubes *Phys. Rev.* B **72** 115411

[42] Schadler L S, Giannaris S C and Ajayan P M 1998 Load transfer in carbon nanotube epoxy composites *Appl. Phys. Lett.* **73** 3842–4

[43] Ruan S, Gao P and Yu T X 2006 Ultra-strong gel-spun UHMWPE fibers reinforced using multiwalled carbon nanotubes *Polymer* **47** 1604–11

[44] Saito R, Takeya T, Kimura T, Dresselhaus G and Dresselhaus M S 1998 Raman intensity of single-wall carbon nanotubes *Phys. Rev.* B **57** 4145–53

[45] Poulin P, Vigolo B and Launois P 2002 Films and fibers of oriented single wall nanotubes *Carbon* **40** 1741–9

[46] Haggenmueller R, Gommans H H, Rinzler A G, Fischer J E and Winey K I 2000 Aligned single-wall carbon nanotubes in composites by melt processing methods *Chem. Phys. Lett.* **330** 219–25

[47] Liu T and Kumar S 2003 Quantitative characterization of SWNT orientation by polarized Raman spectroscopy *Chem. Phys. Lett.* **378** 257–62

[48] Gommans H H, Alldredge J W, Tashiro H, Park J, Magnuson J and Rinzler A G 2000 Fibers of aligned single-walled carbon nanotubes: polarized Raman spectroscopy *J. Appl. Phys.* **88** 2509–14

[49] Chua P S and Piggott M R 1985 The glass fibre—polymer interface: I—theoretical consideration for single fibre pull-out tests *Compos. Sci. Technol.* **22** 33–42

[50] Soumendu B, Abhilash H and Beng C H 2018 Interfacial load transfer mechanisms in carbon nanotube-polymer nanocomposites *Proc. R. Soc. Math. Phys. Eng. Sci.* **474** 20170705

[51] Rubel R I, Ali M H, Jafor M A and Alam M M 2019 Carbon nanotubes agglomeration in reinforced composites: a review *AIMS Mater. Sci.* **6** 756

[52] Rivero P J, Urrutia A, Goicoechea J and Arregui F J 2015 Nanomaterials for functional textiles and fibers *Nanoscale Res. Lett.* **10** 501

[53] Zhou J and Miles R N 2017 Sensing fluctuating airflow with spider silk *Proc. Natl Acad. Sci.* **114** 12120–5